M. SHAHJAHAN,[1,2,3] S.M. TALUKDER,[1] M.S. HOSSAIN,[4] M.H.A. BEGUM,[4]
R.L. WARNOCK,[2,3] M.A. HAQUE,[1] M. HOSSAIN,[5] N.A. AHMED[4]

[1] Department of Physics, University of Chittagong
(Chittagong, Bangladesh)
[2] ENS Paris Saclay
(Paris, France)
[3] Complutense University of Madrid
(Madrid, Spain)
[4] Industrial Physics Division, BCSIR Laboratories Dhaka,
Bangladesh Council of Scientific & Industrial Research (BCSIR)
(Dhaka, 1205, Bangladesh)
[5] Daffodil International University
(Dhaka, 1205, Bangladesh)

SYNTHESIS AND CHARACTERIZATION OF STRUCTURAL, AND ELECTRICAL PROPERTIES OF $Mg_{(0.25x)}Cu_{(0.25x)}Zn_{(1-0.5x)}Fe_2O_4$ FERRITES BY SOL-GEL METHOD

UDC 539

The effects of magnesium, copper, and zinc substitutions on spinel ferrites have been investigated by the sol-gel technique. Ferrite compositions of $Mg_{0.25x}Cu_{0.25x}Zn_{(1-0.5x)}Fe_2O_4$ *(where* $x = 0.6$*, 0.7, 0.8 & 0.9) were prepared at a sintering temperature of 1100 °C with a presintering at 500 °C. X-ray diffraction (XRD), scanning electron microscopy (SEM), and high-precision impedance analysis are used to characterize structural and dielectric properties, as well as the surface topography and morphology of the samples. A single phase, cubic spinel structure, with decreased lattice constant was observed. SEM micrographs revealed a homogeneous microstructure with uniform size distributions. Both the dielectric constant and dielectric loss tangent decrease, as the incident frequency increases up to a certain saturation point. The direct current (dc) resistivity profile shows that the resistivity increases with the temperature up to the Curie point, then it goes to a constant value. The quality factor (Q-factor) increases with the incident frequency. Hence, the high Q-factor will make ferrites highly useful in applications, especially in multilayer chip inductors.*

K e y w o r d s: MgCuZn ferrite, sol-gel method, nanocrystalline ferrites, magnetic properties, multilayer chip inductors.

1. Introduction

Nanocrystalline spinel ferrites have been enormously used in many devices due to their high electrical resistivity, low dielectric losses, high permeability, high Curie temperature (Tc) [1–3], high chemical stability [4], high-density magnetic recording, microwave isolators [5], and low manufacturing cost [4]. Ferrites have shown low eddy current losses and thus are considered superior magnetic materials due to their high electrical resistivity. Though Mg–Cu–Zn ferrites and Ni–Cu–Zn ferrites exhibit the high resistivity and high permeability at high frequencies, Mg–Cu–Zn ferrites have several advantages over Ni–Cu–Zn ferrites. They are more economical [6] and easier to be synthesized. Moreover, Ni-Zn ferrites produce carcinogenic effects and the environmental toxicity due to their nickel content [7]. Because of the excellent characteristics and less adverse effects, there is a growing interest of scientists in Mg–Zn ferrites for using them in electronic devices. One example of such a device that would benefit from the integration of Mg–Cu–Zn ferrites is multilayer chip inductors [8], which might have uses to suppress the noise in high-frequency electrical circuits. Large stainless steel

(S.S.), small S.S. pagers, camera recorders, radios, and cordless telephones can also be applied by these ferrites. Doping with a transition metal such as Cu shows some important influence on the magnetic and electric properties [9–10] of Mg–Zn ferrites. Yue *et al.* [11] studied a $(Mg_{0.5-x}Cu_xZn_{0.5})O_{0.02}(Fe_2O_3)_{0.98}$ ferrites with Cu substitution and observed the improved permeability, where the cutoff frequency was around 10 MHz. Barati *et al.* [12] investigated electromagnetic properties of a $Mg_{0.8-x}Cu_{0.2}Zn_xFe_2O_4$ ferrites whose permeability was improved with an increase in the Zn content, but the frequency stability (2 MHz) was poor. The dielectric behavior of a $Mg_{0.55-x}Cu_xZn_{0.45}O_{0.03}(Fe_2O_3)_{0.97}$ ($x = 0.0 - 0.35$) ferrites was investigated by Haque *et al.* [13] and showed an increase in the permeability due to the Cu substitution, where the maximum relaxation frequency was around 5.7 MHz for $x = 0.2$. In addition, Cu-substituted Mg–Zn ferrites showed the substitution-improved permeability, but the relaxation frequencies were low (on the order of few hundreds of kHz to MHz) [14–16]. One of the objectives of the following research was to improve the relaxation frequency of Mg–Cu–Zn ferrites. Berchmans *et al.* [17] and Naeem *et al.* [18] discussed the cation distribution in a system of Ni–Mg ferrites and found that if the Ni content in the spinel was maximized, the Mg percentage at the tetrahedral site was maximized [19]. Substituting Mg for Ni in Ni–Zn ferrites improved the electric and magnetic properties, as reported by Singh *et al.* [20]. Varalaxmi *et al.* [21] studied the substitution of Mg in Ni–Cu–Zn ferrites and found an improvement of the initial permeability and a reduction of the Curie temperature (T_c). Roy *et al.* [22] investigated the electromagnetic properties of Ni–Cu–Zn ferrites by the Mg doping and found that, up to a fixed concentration of Mg, the electric resistivity and initial permeability both are increased. Hence, the area of a recent interest in research with nanoferrites is growing in their synthesis part. They have potential applications in different technological areas like the targeted drug delivery, medical imaging, biomedical applications, magnetic data storage, and ferrofluids [23–27]. In order to be applied successfully in applications, nanoferrites with uniform size distributions are desirable. The magnetic property of these nano-sized ferrites goes completely different from their bulk counterparts [28]. If the diameter of nanoparticles is smaller than the critical diameter, the multidomain formation and hindering domain wall motion can be avoided, as the increasing domain wall decreases the magnetization. In addition, the wall size is affected with the demagnetization of ferrites. Here, the magnetization of single-domain particles is due to the rotation of a spin which can improve the material operating frequency. Again, the spin rotation is in the GHz frequency region [29], which is useful in biomedical applications as well. Nanosized Mg–Cu–Zn ferrites can be prepared by various wet chemical methods, including the citrate method [30–31], chemical co-precipitation method [32], sol-gel technique [33], combustion synthesis [34–35], and hydrothermal synthesis [36]. The foremost advantage of the sol-gel auto-combustion process is the nanoscale yield without the use of an expensive equipment [37]. A comparative study among all the preparation techniques gives the idea that the sol-gel autocombustion method has clear advantages over the other methods. It is possible to produce highly crystalline and uniform nanopowders without applying the high energy. Technically, this technique is simple and easy to conduct experiment. Moreover, the sol-gel method has direct influence on the sintering temperature, anneling time, doping concentration, and pH of the solution, which controls the electrical and structural properties of ferrites.

In this research, the samples of ferrites were firstly presintered at 500 °C and then sintered at a high temperature of 1100 °C. Structural, morphological, and dielectric properties were investigated and analyzed for the first time in the configuration of ferrites described below. Only the optimum findings which will be important for their application are presented.

2. Materials and Method

Analytical grade $Mg(NO_3)_2{\cdot}6H_2O$, $Cu(NO_3)_2{\cdot}3H_2O$, $Zn(NO_3)2.4H_2O$ and $Fe(NO_3)_3{\cdot}9H_2O$ were used as raw materials for the samples of Mg–Cu–Zn ferrites with the formula $Mg_{(0.25x)}Cu_{(0.25x)}Zn_{(1-0.5x)}Fe_2O_4$, (where $x = 0.6, 0.7, 0.8, 0.9$). The required amount of metal nitrate and a citric acid solution was mixed in a beaker keeping the molar ratio 1:1 of nitrates to citric acid. At first, all the salts of metals were mixed in a beaker, and the solutions were prepared by adding properly distilled water. After that, the citric acid solution was placed on the previously prepared solution dropwise. During the droping, the solution was under

continuous strring for getting a homogeneous mixture solution. The pH of the solution was carefully adjusted and fixed to 7 using required ammonia solutions. At the same time, the solution was rigorously stirred by a magnetic stirr bar during the entire procedure. Then the solution was heated up to 200 °C on a hotplate. After 30 min of the heating, it is observed that the stirring solution is transformed into a concentrated viscous gel. At 200 °C, the gel is ignited and burns out in a self-propagating combustion manner and turns into a loose powder. The whole combustion process finished within a short time. The powder was collected and and pestled for getting a fine powder. Finally, the calcinations of the collected burnt powders have done at 500 °C using a programmable furnace for 1 h for getting single phase ferrites. The granulation of the calcite powders has been done using a 1% saturated solution of polyvinyl alcohol as a binder. The stainless steel die is used to form pellets applying the fixed pressure by a digital press machine. A programmable muffle furnace is used for the sintering at 1100 °C for 6 h. The specimen surface was polished to remove oxide or other extra layers which are formed during the sintering. Finally, the pellets were coated with a silver paint for next measurements.

3. Results and Discussion

3.1. Structural properties

Figure 1 shows the X-ray diffraction patterns of the samples. An X-ray powder diffractometer by Bruker was used for the identification of crystalline phases using $\lambda(\text{Cu–K}_\alpha) = 1.5406$ Å with a step size of 0.02, $2\theta°$ at room temperature. Structural parameters of the spin phases and the lattice constant were determined using the X-ray diffraction patterns. Atomic positions for the spinel phase and the structural parameters were obtained from the literature sources. XRD patterns and the presence of all the peaks belonging to the cubic spinel structure proved that the formed samples have single phases. The lattice constant a was found using the formula

$$a = d_{hkl}\sqrt{h^2 + k^2 + l^2}, \tag{1}$$

where h, k, l are the Miller indices, and d_{hkl} is the interplanar spacing.

The highest intensity peak is at the 35 °C position which is (311) plane. This proves that the spinel ferrites are formed. The average crystallite sizes of the bulk samples (D_p) were calculated using the Scherrer formula

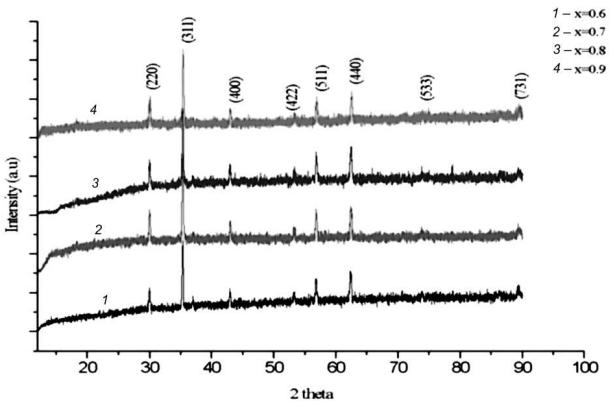

Fig. 1. XRD patterns for $\text{Mg}_{(0.25x)}\text{Cu}_{(0.25x)}\text{Zn}_{(1-0.5x)}\text{Fe}_2\text{O}_4$ ($x = 0.6, 0.7, 0.8, 0.9$) ferrites

$$D_p = \frac{0.94\lambda}{\beta\cos\theta}, \tag{2}$$

where the line broadening in radians is β, Bragg angle θ, and the X-ray wavelength is λ.

It is observed that the crystal size reduces with a decrease in the Zn content shown in Table 1, since a Zn atom is larger than the Cu and Mg atoms, which matches exactly with the available theory. Table 1 contains the structural parameters measured from the XRD graphs for the cation concentration. All the sintered ferrites showed almost same lattice constant (a), but there is a a tendency to reduce the value, as the cation concentration increases.

The X-ray density was calculated using the formula

$$\rho_{\text{ferrite}} = \Sigma\frac{8M}{Na^3}, \tag{3}$$

where M is the molecular weight, N is Avogadro's number, and "a" is the lattice constant. The bulk density of the circularly shaped sample was calculated using the formula

$$d_{\text{Bulk}} = \frac{\text{mass}}{\pi r^2 t}, \tag{4}$$

where r and t are the pellet radius and thickness, respectively. Using the Archimedean porosimetry concept from the bulk density and X-ray theoretical density, the porosity percentage (%P) was calculated and tabulated. We also checked the presence of a porosity from the SEM image manually and got its small

Table 1. **Some structural parameters of $Mg_{(0.25x)}Cu_{(0.25x)}Zn_{(1-0.5x)}Fe_2O_4$ ($x = 0.6$, 0.7, 0.8, 0.9) ferrites**

Sample composition	Crystallite size (nm)	Lattice constant (Å)	X-Ray densiti (ρx) g cm^{-3}	Bulk densiti (ρa) g cm^{-3}	% (P)
$Mg_{0.15}Cu_{0.15}Zn_{0.70}Fe_2O_4$	26.29	8.4220	5.2169	4.4749	14.22
$Mg_{0.175}Cu_{0.175}Zn_{0.65}Fe_2O_4$	25.19	8.4188	5.1989	4.2799	17.67
$Mg_{0.20}Cu_{0.20}Zn_{0.60}Fe_2O_4$	24.21	8.4174	5.1776	4.3421	16.13
$Mg_{0.225}Cu_{0.225}Zn_{0.55}Fe_2O_4$	23.7	8.4098	5.1677	4.3385	16.04

value. Here, the lattice constant decreases, as the Cu and Mg contents increase and the Zn content decreases. This is due to a larger ionic radius of Cu^{2+} compared to Mg^{2+}, while the concentration of Zn_{2+} ions in the samples decreases. The bulk density decreases, except for the $x = 0.7$ sample, with a decrease in the Zn^{2+} concentration, because of a large atomic weight of Zn as compared with Cu and Mg atoms (see Table 1). At $x = 0.7$, the bulk density is the lowest, may be, for the same amount of Cu and Mg in the samples, which makes difficulties for the formation of ferrites and consequently reduces the density. The lowest density gives high porosity. Hence, the $x = 0.7$ sample gives the highest porosity for the same reason. Decreasing the bulk density with decreasing the Zn content due to the addition of Cu and Mg improves the densification and decreases the porosity as well. The bulk density is highest at $x = 0.6$, and, consequently, the porosity is the lowest due to a high density. The density calculated by X-ray data (ρ_x) reduces from 5.21 g/cm^3 to 5.16 g/cm^3 with increasing the Cu and Mg contents. Moreover, the X-ray density is inversely dependent on the lattice parameters. Thus, the respective X-ray density decreases with increasing the Cu and Mg contents. Barati, *et al.* reported a similar result for Mg–Cu–Zn ferrites [12], where the close aggrement and correlation exists among the observed bulk density, X-ray density, and porosity for the ferrites sintered at 1100 °C. It was observed that the X-ray densities were larger than the bulk densities, because of the existence of pores. Table 1 clearly shows that, with increasing the Cu content, the porosity percentage decreases, as expected, because of the above reason. This porosity trend is the identical characteristic of good-quality ferrites, since the physical properties of ferrites also depend on the porosity.

3.2. Morphology

Scanning Electron Microscopy (SEM) has been employed to examine the nanostructural features shown in Fig. 2. The high-resolution SEM could measure the surface morphology. The grain size was obtained by the method of line intercept [40] from SEM micrographs; this method resulted in the average grain size given in Table 2. As seen in Fig. 2, the SEM micrographs show a homogeneous microstructure with uniform small-size distribution, where some cavities on the surface may be due to the evaporation of Zn ions from the crystal [41].

The grain size is measured from the SEM images using the ImajeJ software. It decreases with decreasing the Zn content and increasing the Cu and Mg contents except for $x = 0.9$ (see Table 2). At $x = 0.9$, the grain size increases, because the Cu content is the highest there. It is observed that the crystalline grain size from the Scherrer equation is smaller than the average grain size from the SEM micrographs, which follows the result in [42].

3.3. Measurements of electrical properties

3.3.1. Variation of d.c. resistivity with temperature

The d.c. electrical resistivity (ρ) of the samples was calculated by the two-probe method.

The Curie temperature is determined from the measurement of the resistivity as a function of the temperature using the curve of $\ln \rho$ versus $1000/T$ at the point of the phase transition from the ferromagnetic to paramagnetic phase. The temperature-dependent d.c. electrical resistivity was measured using the formula

$$R = \rho l/A \quad \text{or} \quad \rho = RA/l, \tag{5}$$

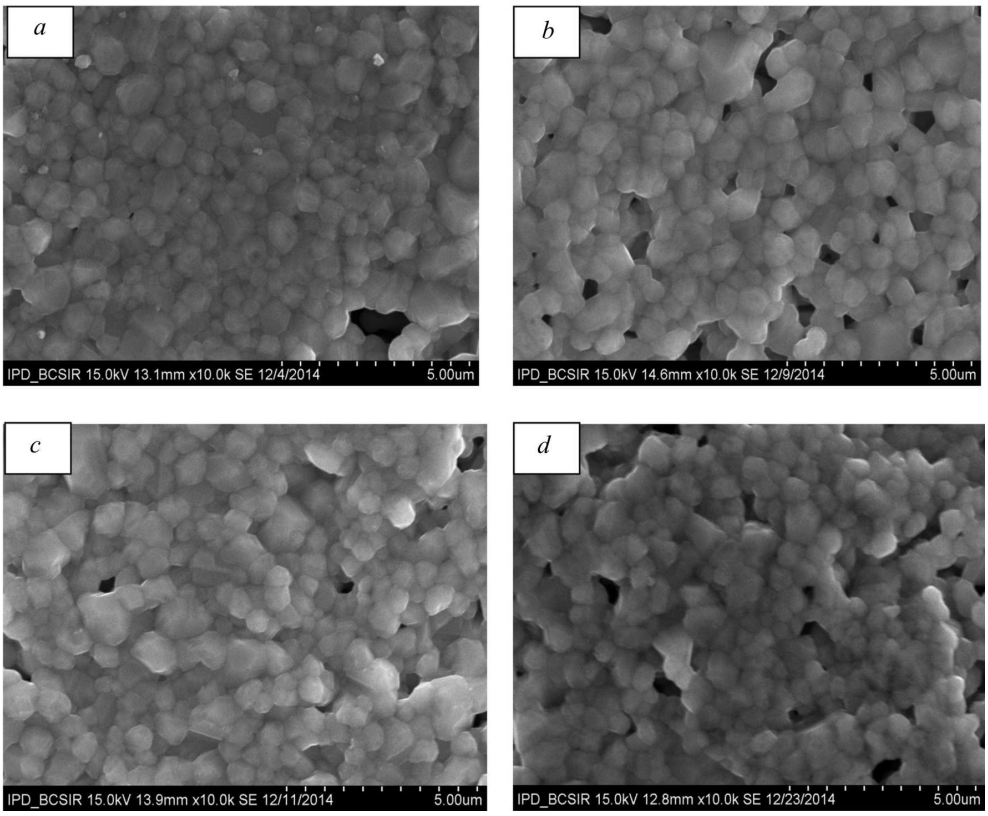

Fig. 2. Scanning electron micrographs of $Mg_{0.25x}Cu_{0.25x}Zn_{(1-0.5x)}$ Fe_2O_4 $x = 0.6$ (a), $x = 0.7$ (b), $x = 0.8$ (c), $x = 0.9$ (d) ferrites

Table 2. **Some parameters of $Mg_{0.25x}Cu_{0.25x}Zn_{(1-0.5x)}$ Fe_2O_4 ($x = 0.6, 0.7, 0.8, 0.9$) ferrites**

Composition	Grain D nm (average d)	Resistivity $\rho(\Omega - m)$ at normal temperature	Transition temperature T_c (°C)	Resistivity $\rho(\Omega - m)$ at T_c
$Mg_{0.15}Cu_{0.15}Zn_{0.70}Fe_2O_4$	517	65837.23	100	12392.55
$Mg_{0.175}Cu_{0.175}Zn_{0.65}Fe_2O_4$	505	78482.02	150	4101.437
$Mg_{0.20}Cu_{0.20}Zn_{0.60}Fe_2O_4$	500	101593.21	130	2876.85
$Mg_{0.225}Cu_{0.225}Zn_{0.55}Fe_2O_4$	526	29714.81	240	52.94

where A is the cross-section area of the sample, l is the thickness of the sample, and R is the resistance of the sample given by $R = (V_s/V_s) \times R_f$. Hence, from the above equations, we have

$$\rho = AR_f/l(V_s/V_f). \tag{6}$$

Here, V_s is the voltage across the sample, and V_f is the voltage across the fixed resistance R_f. By using the above equations, the d.c. resistivity can be determined [43].

The d.c. resistivity (ln) curves for the samples have been plotted versus the temperature ($1000/T$) and the frequency, as shown in Figs. 3 and 4. From these plots, it is observed that the d.c. resistivity decreases with increasing the temperature up to a certain value and with increasing the frequency as well. At the fixed-point temperature, the resistivity becomes saturated and is not changed with increasing the temperature. In this case, the Curie temperatures (T_C) of all four samples at a sintering temperature of

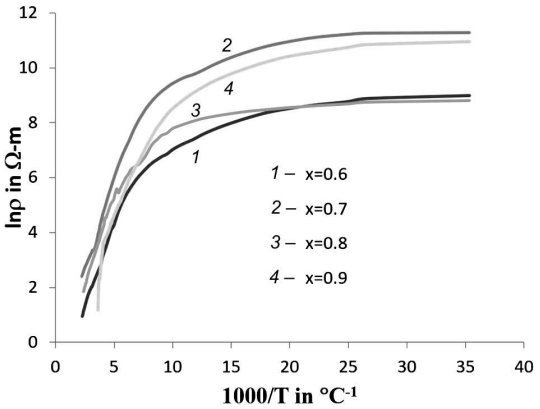

Fig. 3. Resistivity ($\ln \rho$) vs temperature ($1000/T$) graphs of $Mg_{0.25x}Cu_{0.25x}Zn(1-0.5x)Fe_2O_4$ (x = 0.6, 0.7, 0.8, 0.9) ferrites

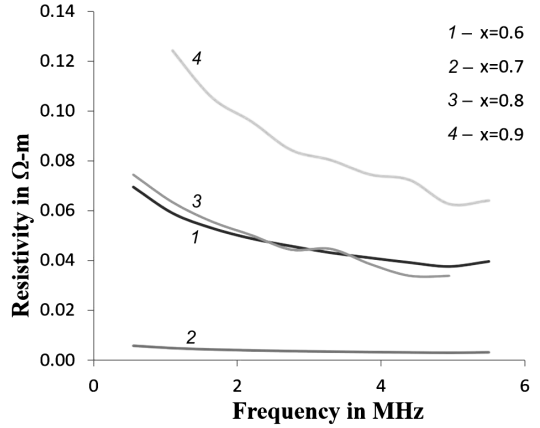

Fig. 4. Frequency-dependent resistivity for the sintered $Mg_{0.25x}Cu_{0.25x}Zn(1-0.5x)Fe_2O_4$ (x = 0.6, 0.7, 0.8, 0.9) ferrites

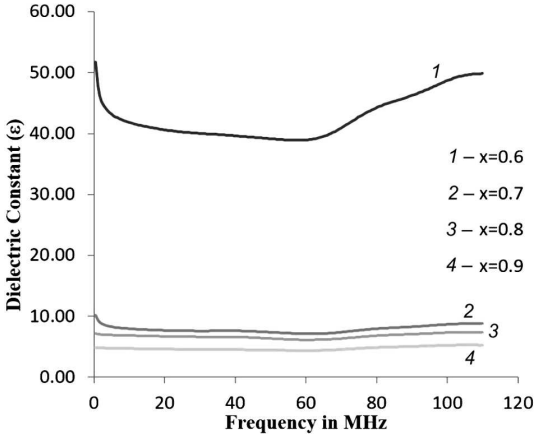

Fig. 5. Frequency-dependent dielectric constant for the sintered $Mg_{0.25x}Cu_{0.25x}Zn(1-0.5x)Fe_2O_4$ (x = 0.6, 0.7, 0.8, 0.9) ferrites

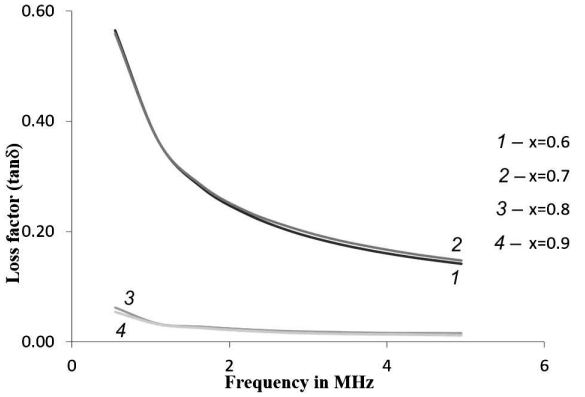

Fig. 6. Frequency-dependent dielectric loss tangent for the sintered $Mg_{0.25x}Cu_{0.25x}Zn(1-0.5x)Fe_2O_4$ (x = 0.6, 0.7, 0.8, 0.9) ferrites

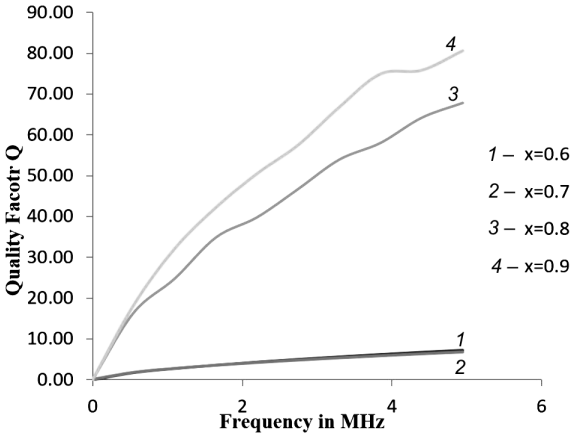

Fig. 7. Frequency-dependent quality factor for the sintered $Mg_{0.25x}Cu_{0.25x}Zn(1-0.5x)Fe_2O_4$ (x = 0.6, 0.7, 0.8, 0.9) ferrites

1100 °C were 100 °C, 150 °C, 130 °C, and 240 °C, respectively.

The frequency response of the d.c. resistivity at room temperature is the highest at $x = 0.9$ due to increasing the Mg content, since a Mg atom has a lower electrical conductivity than Cu and Zn ones. At $x = 0.9$, the Mg content is the highest here, and the Zn content is the lowest. That is why this composition has a high resistivity and hence the lowest conductivity. At $x = 0.7$, we see the lowest resistivity at the same amount of Cu and Zn. Hence, the Cu content has the leading role as compared with Mg, by increasing the conductivity and, consequently, decreasing the resistivity. But the transition temperature and the resistivity at the transition point in-

crease with x values, i.e., with increasing the Mg and Cu contents and decreasing the Zn content.

4. Dielectric Properties

The results of frequency-dependent room-temperature dielectric measurements are shown in Fig. 5. The formula for dielectric constant is

$$\varepsilon_0' = \frac{C_p t}{{}_0 A}, \tag{7}$$

where the disc-shaped pellet parallel capacitance is C_P (in pF), thickness of a pellet is t, and the cross-section area of the flat surface is A. Dielectric properties are dependent on the technique of preparation, especially on the chosen conditions.

Figure 5 shows the effect of different reactant concentrations on the frequency-dependent dielectric constant. It is found that it follows the general trend of ferroelectrics [38], where the dielectric constant decreases with increasing the frequency. Figure 5 shows also that the dielectric constant decreases with increasing the frequency for all samples continuously and reaches a fixed value at a frequency of 65 MHz. For the sample with $x = 0.6$, the dielectric constant is significantly higher than for other samples because of a higher Zn content in the samples. This value is not competable with the general properties of ferrites just because of a high Zn content. Again, after the frequency of 65 MHz, the dielectric constant increases with the frequency because of the oriential polarization at higher frequencies. Hence, reducing the eddy current at high-frequency applications is possible, by using the observed low dielectric constant behavior [39].

The dielectric loss tangent ($\tan\delta$) variation with the frequency is shown in Fig. 6. The value of $\tan\delta$ depends on various factors like the stoichiometry, Fe^{2+} content, and homogeneity of a structure. Losses are the highest for a low Mg content, which decrease with increasing the frequency. The Q-factor as a function of the frequency is shown in Fig. 7. The Q-factor increases with the concentration of Mg and Cu contents, and, consequently, as the Zn content decreases. The Q-factor increases with the frequency so that the prepared samples would be used for high-frequency applications. Among the samples, the sample with $x = 0.9$ shows the maximum Q-factor equal to 75.89.

5. Conclusion

The present investigation has done using $Mg_{0.25x}Cu_{0.25x}Zn_{(1-0.5x)}Fe_2O_4$ (where $x = 0.6, 0.7$, 0.8 and 0.9) ferrites. All samples were prepared by the sol-gel technique. The chemical composition of these synthesized ferrite samples influences the structural and electrical properties of these materials. The d.c. resistivity decreases and goes to the saturation point at the Curie temperature (T_C) with increasing the temperature and the frequency as well. Both the dielectric constant and loss factor have decreasing trends with increasing the frequency. It is found that the d.c. electrical resistivity and the dielectric and nanostructural properties of prepared ferrites are influenced significantly by changing the temperature and the cation concentrations. The graphs of the dielectric loss tangent and quality factor versus the frequency allow us to find the best composition. The sample at $x = 0.9$ has the maximum Q-factor as high as 75.89, which clearly represents the best composition among all. Increasing the Mg content and decreasing the Zn content make high-quality ferrites which are capable to response to high-frequency applications. Hence, we may conclude that the nano-sized synthesized sintered ferrite at $x = 0.9$ ($Mg_{0.225}Cu_{0.225}Zn_{0.55}Fe_2O_4$) is highly active and have high quality which might be suitable for multilayer chip inductor applications.

We would like to express our grateful thanks and gratitude to the authorities of the University of Chittagong and BCSIR Laboratories, Dhaka for providing us the opportunity and the necessary permission to carry out this research work. Thanks are also due to all the employees of the Industrial Physics Division at BCSIR Laboratories, Dhaka.

1. Z. Yue, J. Zhou, L. Li, X. Wang, Z. Gui. Effect of copper on the electromagnetic properties of Mg–Zn–Cu ferrites prepared by sol-gel auto-combustion method. *Mat. Sci. Eng. B* **86**, 64 (2001).
2. X. Qi, J. Zhou, Z. Yue, Z. Gui, L. Li. Effect of Mn substitution on the magnetic properties of MgCuZn ferrites. *J. Mag. Mag. Mat.* **251**, 316 (2002).
3. Z.B. Yue, J.B. Zhou, X.B. Wang, Z.B. Gui, L.B. Li. Low-temperature sintered Mg–Zn–Cu ferrite prepared by auto-combustion of nitrate-citrate gel. *J. Mat. Sci. Lett.* **20**, 1327 (2001).
4. D.S. Mathew, R.S. Juang. An overview of the structure and magnetism of spinel ferrite nanoparticles and their synthesis in microemulsions. *Chem. Eng. J.* **129**, 51 (2007).

5. E. Manova, B. Kunev, D. Paneva, I. Mitov, L. Petrov. Mechano-synthesis, characterization, and magnetic properties of nanoparticles of cobalt ferrite, $CoFe_2O_4$. *Chem. Mat.* **16**, 5689 (2004).
6. P.J. Hak, K.J. Ho, C.S. Hee. *Proceedings of the Seventh International Conference on Ferrites* (Bordeaux, France, 1996).
7. A. Daigle, J. Modest, A.L. Geiler, S. Gillette, Y. Chen, M. Geiler, B. Hu, S. Kim, K. Stopher, C. Vittoria, V.G. Harris. Structure, morphology and magnetic properties of $Mg_{(x)}Zn_{(1-x)}Fe_2O_4$ ferrites prepared by polyol and aqueous co-precipitation methods: A low-toxicity alternative to $Ni_{(x)}Zn_{(1-x)}Fe_2O_4$ ferrites. *Nanotechnology* **22**, 305708 (2011).
8. M.P.l Reddy, W. Madhuri, N.R. Reddy, K.V. Siva Kumar, V.R.K. Murthy, R.R. Reddy. Influence of copper substitution on magnetic and electrical properties of MgCuZn ferrite prepared by microwave sintering method. *Mat. Sci. Eng.* **30**, 1094 (2010).
9. R. Hobne, K. Melzer, H. Hochschild, G. Libor, R. Krause. Magnetic after-effects in titanium-doped magnetite. *Phys. Staus Solidi A* **27**, 117 (1975).
10. A.H. Wafik, S.A. Mazen, S.F. Mansour. Composition dependence of discontinuous magnetization in Li–Ti ferrites. *J. Phys. D: Appl. Phys.* **26**, 2010 (1993).
11. Z. Yue, J. Zhou, L. Li, X. Wang, Z. Gui. Effect of copper on the electromagnetic properties of Mg–Zn–Cu ferrites prepared by sol-gel auto-combustion method. *Mat. Sci. Eng. B* **86**, 64 (2001).
12. M.R. Barati. Influence of zinc substitution on magnetic and electrical properties of MgCuZn ferrite nanocrystalline powders prepared by sol-gel auto-combustion method. *J. Alloys and Compounds* **478**, 375 (2009).
13. M.M. Haquea, M. Huqa, M.A. Hakim. Densification, magnetic and dielectric behaviour of Cu-substituted Mg–Zn ferrites. *Mat. Chem. Phys.* **112**, 580 (2008).
14. Z. Yue, J. Zhou, L. Li, X. Wang, Z. Gui. Effect of copper on the electromagnetic properties of Mg–Zn–Cu ferrites prepared by sol-gel auto-combustion method. *Mat. Sci. Eng. B* **86**, 64 (2001).
15. M.M. Haquea, M. Huqa, M.A. Hakim. Densification, magnetic and dielectric behaviour of Cu-substituted Mg–Zn ferrites. *Mat. Chem. Phys.* **112**, 580 (2008).
16. J. Murbe, J. Topfer. Mg–Cu–Zn ferrites for multilayer inductors. *Int. J. App. Ceramic Technol.* **4**, 415 (2007).
17. L.J. Berchmans, R. Kalai Selvana, P.N. Selva Kumar, C.O. Augustin. Structural and electrical properties of $Ni_{1-x}Mg_xFe_2O_4$ synthesized by citrate gel process. *J. Mag. Mag. Mat.* **279**, 103 (2004).
18. M. Naeem, N.A. Shah, I.H. Gul, A. Maqsood. Structural, electrical and magnetic characterization of Ni–Mg spinel ferrites. *J. Alloys and Compounds* **487**, 739 (2009).
19. V.K. Mittal, P. Chandramohan, S. Era, M.P. Srinivasan, S. Velmurugan, S.V. Narasimhan. Cation distribution in $Ni_xMg_{1-x}Fe_2O_4$ studied by XPS and Ḿossbauer spectroscopy. *Sol. Stat. Commun.* **137**, 6 (2006).
20. N. Singh, A. Agarwal, S. Sanghi, P. Singh. Effect of magnesium substitution on dielectric and magnetic properties of Ni–Zn ferrite. *Phys. B: Cond. Matter* **406**, 687 (2011).
21. N. Varalaxmi, N.R. Reddy, M.V. Ramana, E. Rajagopal, V.R. Murthy, K.V. Sivakumar. Stress sensitivity of inductance in NiMgCuZn ferrites and development of a stress insensitive ferrite composition for microinductors. *Mat. in Electron.* **19**, 399 (2008).
22. P.K. Roy, J. Bera. Effect of Mg substitution on electromagnetic properties of $(Ni_{0.25}Cu_{0.20}Zn_{0.55})Fe_2O_4$ ferrite prepared by auto combustion method. *J. Mag. Mag. Mater.* **298**, 38 (2006).
23. M. Shinkai. Functional magnetic particles for medical application. *J. Biosci. Bioeng.* **94**, 606 (2002).
24. A.S. Lubbe, C. Alexiou, C. Bergemann. Clinical applications of magnetic drug targeting. *J. Surgical Res.* **95**, 200 (2001).
25. L.X. Tiefenauer, A. Tschirky, G. Kuhne, R.Y. Andres. In vivo evaluation of magnetite nanoparticles for use as a tumor contrast agent in MRI. *Mag. Res. Imaging* **14**, 391(1996).
26. R. Skmoski. Nanomagnetics. *J. Phys.: Cond. Matter* **15**, 841 (2003).
27. M.R.J. Gibbs. Nanomagnetism–nascent or fully formed. *Cur. Opi. Sol. Stat. Mat. Science* **7**, 83 (2003).
28. M.R. Barati. Characterization and preparation of nanocrystalline MgCuZn ferrite powders synthesized by sol-gel auto-combustion method. *J. of Sol-Gel Sci. & Technol.* **52**, 171 (2009).
29. C.H. Sujatha, K.V.l Reddy, K.S. Babu, A.R.C. Reddy, K.H. Rao. Effects of heat treatment conditions on the structural and magnetic properties of MgCuZn nano ferrite. *Ceramics Intern.* **38**, 5813 (2012).
30. M.M. Bahout, S. Bertrand, O. Pena. Synthesis and characterization of $Zn_{1-x}Ni_xFe_2O_4$ spinels prepared by a citrate precursor. *J. Sol. Stat. Chem.* **178**, 1080 (2005).
31. A. Verma, T.C. Goel, R.G. Mendiratta, P. Kishan. Magnetic properties of nickel-zinc ferrites prepared by the citrate precursor method. *J. Mag. Mag. Mater.* **208**, 13 (2000).
32. Q. Chen, A.J. Rondinone, B.C. Chakoumakos, Z. Zhang. Synthesis of superparamagnetic $MgFe_2O_4$ nanoparticles by coprecipitation. *J. Mag. Mag. Materials* **194**, 1 (1999).
33. D.H. Chen, X.R. He. Synthesis of nickel ferrite nanoparticles by sol-gel method. *Mat. Research Bulletin* **36**, 1369 (2001).
34. C.C. Hwang, J.S. Tsai, T.H. Huang. Combustion synthesis of Ni–Zn ferrite by using glycine and metal nitrates-investigations of precursor homogeneity, product reproducibility, and reaction mechanism. *J. Mater. Chem. Phys.* **93**, 330 (2005).
35. C.H. Peng., C.K. Hwang, S.Y. Chen. A self-propagating high-temperature synthesis method for Ni-ferrite powder synthesis. *J. Mater. Sci. Eng. B* **107**, 295 (2004).

36. X. Jiao, D. Chen, Y. Hu. Hydrothermal synthesis of nanocrystalline $M_xZn_{1-x}Fe_2O_4$ (M = Ni, Mn, Co; x = 0.40–0.60) powders. *Mat. Research Bulletin* **37**, 1583 (2002).
37. S.S. Kamble, S.J. Vrushali, P.C. Pingale. Synthesis of $Mg_{0.48}Cu_{0.12}Zn_{0.40}Fe_2O_4$ ferrite and its aptness for multilayer chip component application. *Ceramics Intern.* **39**, 3597 (2013).
38. D. Ravinder, K.V. Kumer. Dielectric behaviour of erbium substituted Mn–Zn ferrites. *Bul. Mat. Sci.* **24**, 505 (2001).
39. M. Sorescua, L. Diamandescua, R. Peelamedu, R. Roy, P. Yadoji. Structural and magnetic properties of NiZn ferrites prepared by microwave sintering. *J. Mag. Mag. Mater.* **279**, 195 (2004).
40. B. Roebuck, C. Phatak, I. Birks-Agnew I. A comparison of the linear intercept and equivalent circle methods for grain size measurement in WC/Co hardmetals. *NPL Report MATC(A)* **149**, (2004).
41. M.F. Huq, D.K. Saha, R. Ahmed, Z.H. Mahmood. Ni–Cu–Zn ferrite research: A brief review. *J. Sci. Res.* **5**, 215 (2013).
42. C. Rath, S. Anand, R.P. Das. Dependence on cation distribution of particle size, lattice parameter, and magnetic properties in nanosize Mn–Zn ferrite. *J. Appl. Phys. B* **91**, 2211 (2002).
43. Y. Singh. Electrical resistivity measurements: A review. *Int. J. Mod. Phys.: Conf. Series* **22**,745 (2013).

Received 25.12.18

М. Шаджахан, С.М. Талукдер,
М.С. Хоссен, М.Х.А. Бегум, Р.Л. Варнок,
М.А. Хак, М. Хоссен, Н.А. Ахмед

СИНТЕЗ І ХАРАКТЕРИСТИКА СТРУКТУРИ І ЕЛЕКТРИЧНИХ ВЛАСТИВОСТЕЙ $Mg_{(0,25x)}Cu_{(0,25x)}Zn_{(1-0,5x)}Fe_2O_4$ ФЕРИТІВ ЗОЛЬ-ГЕЛЬ МЕТОДОМ

Р е з ю м е

Із використанням золь-гель методу вивчені ефекти від добавок магнію, міді і цинку на феритах шпінелі. Ферити складу $Mg_{0,25x}Cu_{0,25x}Zn_{(1-0,5x)}Fe_2O_4$ (де x = 0,6, 0,7, 0,8 & 0,9) виготовлені при температурі спікання 1100 °C з попереднім нагріванням при 500 °C. Використано рентгеноструктурний аналіз, растрову електронну мікроскопію (РЕМ) і високоточний імпедансний аналіз для визначення структури, діелектричних властивостей, топографії поверхні і морфології зразків. РЕМ-зображення показують однорідну мікроструктуру з однорідним розподілом розмірів. Діелектрична константа і тангенс діелектричних втрат зменшуються з ростом зовнішньої частоти до певної точки насичення. Опір за постійним током зростає з температурою до точки Кюрі, де виходить на постійне значення. Q-фактор зростає з частотою, що робить ферити дуже корисними на практиці, зокрема, в багатошарових котушках індуктивності чіпів.